

Joint Centre for Mesoscale Meteorology, Reading, UK



Radiation and Polar Lows

G. C. Craig

Internal Report No. 25

February 1994

Met Office Joint Centre for Mesoscale Meteorology Department of Meteorology
University of Reading PO Box 243 Reading RG6 6BB United Kingdom
Tel: +44 (0)118 931 8425 Fax: +44 (0)118 931 8791
www.metoffice.com



Radiation and Polar Lows

George C. Craig

**Joint Centre for Mesoscale Meteorology
Department of Meteorology
University of Reading**

February 18, 1994

SUMMARY

In axisymmetric simulations of a convective polar low, it was found that long-wave radiative cooling increases both growth rate and maximum intensity. This result was due to cooling of the system's environment relative to its warm core. The magnitude of the increase in growth rate was approximately 30%, but was sensitive to the parameterization of cloud microphysics and radiative properties. A steady-state Carnot cycle was not obtained.

1. INTRODUCTION

At first glance, it seems unlikely that radiation would be of great importance for polar lows. Radiative heating and cooling of the atmosphere are certainly important over periods of several days, but a polar low will often evolve from first detection to maximum intensity in less than twenty-four hours. However, it has been shown that radiative effects significantly modulate the behavior of many convective weather systems, including midlatitude squall lines (Chen and Cotton 1988), tropical convective clusters (Dudhia 1989), and tropical cyclones (Kurihara and Tuleya 1981, Hack 1980). To the extent that the structure and evolution of polar lows are determined by convection, they may be influenced by radiation in a similar manner.

The presence of organized cumulus convection in polar lows is a characteristic feature, but the extent of its role has been the subject of some debate (Harold and Browning 1969, Rasmussen 1979, 1983, Reed 1979, Craig and Cho 1988, 1992b). Recent observational work describes a variety of polar low types, including some believed to be driven largely by diabatic heating (Lystad 1986, Businger and Reed 1989). Extreme cases show a number of similarities to tropical cyclones (Rasmussen 1989, Nordeng and Rasmussen 1992), where radiative effects are known to be important.

Most work on the effects of radiation on tropical convective systems has focused on two mechanisms: large-scale destabilization of the troposphere by long-wave cooling, and preferential cooling of cloud-free areas surrounding the convective region (Miller and Frank 1993, and refs.). In the first process, mean cooling of the troposphere in relation to the underlying surface helps to destabilize the atmosphere and enhance convection (eg. Dudhia 1989). The second process relies on horizontal gradients of heating, rather than just the average value. Cooling of clear air relative to cloudy regions leads to enhanced subsidence and convergence at low levels into the convective area (Gray and Jacobson 1977). Both mechanisms are modulated by the diurnal cycle since solar heating during daylight hours reduces the mean tropospheric cooling and reduces or even reverses the horizontal gradients of heating and cooling. The growth of convective polar lows may be affected by both mechanisms, but the diurnal cycle is likely to be less important due to the weakness of solar heating in the arctic winter. In addition, the large air-sea temperature differences in the cold air outbreaks where the polar lows typically form act strongly to destabilize the atmosphere, and may make the convection less sensitive to subtle changes in tropospheric cooling rates.

The effect of radiation on polar lows is also of theoretical interest. Emanuel and Rotunno

(1989) suggested that a polar low could be represented as a Carnot heat engine, in a manner similar to that previously proposed for tropical cyclones (Emanuel 1986, Rotunno and Emanuel 1987). In this conceptual model, a working fluid, moist air, undergoes a thermodynamic cycle consisting of warming and moistening at the sea surface as it spirals in towards the centre of the polar low, moist adiabatic ascent near the radius of maximum winds, and radiative cooling in the upper troposphere, followed by adiabatic descent back to the sea surface. By equating the work done in this cycle to the loss of energy due to surface friction, Emanuel and Rotunno constructed a steady-state model of the mature polar low which gave predictions for the minimum central pressure in terms of the sea surface temperature and the mean temperature of the outflow near the tropopause. These predictions were found to compare favourably with observations and output from a numerical model.

A principal problem with applying the Carnot cycle model to atmospheric weather systems is that the working fluid does not follow a closed cycle. The air converging into the polar low at low levels is generally not air that flowed out at upper levels, and does not necessarily have the same thermodynamic properties that would have resulted from subsidence in response to radiative cooling. Even the numerical model of Rotunno and Emanuel does not represent the Carnot cycle exactly since radiation is ignored [the tropical cyclone simulations of Rotunno and Emanuel (1987) employed a simple Newtonian cooling]. It can nonetheless be hypothesized that if an isolated polar low were to occur, surrounded by a relatively benign environment consisting perhaps of disorganized convection, a circulation close to the idealized Carnot cycle might be observed. If such a system could be constructed in a numerical model with realistic treatment of radiative and convective processes, it would provide a good laboratory for examining the utility of the conceptual model.

This paper describes numerical simulations of a convective polar low with detailed calculation of longwave radiative cooling, on a domain large enough to include both the vortex and its environment. To minimize the difficulties associated with the parameterization of cumulus convection, a cloud-resolving model is used. This allows explicit calculation of the distributions of water vapour and cloud ice, which are crucial to the determination of radiative fluxes.

The simulations are carried out on a two-dimensional, axisymmetric domain. While the assumption of two-dimensionality is quite restrictive, examples of polar lows exist which are nearly axisymmetric in the mature stages (Businger and Baik 1991, Nordeng and Rasmussen 1992). This suggests that a two-dimensional representation of the polar low is reasonable, provided that one ignores the early stages of the simulation, before the vortex is well-established. The structure of the convection

in the environment is less important, since only the average thermodynamic properties of the atmosphere such as temperature, moisture content, and cloud fraction are likely to influence the polar low. Comparison of two and three dimensional cloud simulations with observations by Tao et al. (1987) indicated that the two-dimensional simulations provided reasonable predictions of average properties of the cloud ensemble in situations where the convection was observed to be two-dimensional. Although this is not always the case, linear convective organization is sometimes observed in polar air outbreaks (Businger and Walter 1988), suggesting that the axisymmetric model will provide at least a physically plausible description of the environment. While three-dimensional simulations would clearly be desirable, there are equally large uncertainties associated with the parameterizations of cloud microphysics and radiative properties, as will be discussed later.

In section 2, a brief description of the numerical model is provided. Section 3 gives the results of experiments to delineate the effects of radiation on the growth rate and intensity of the polar low, while section 4 describes the long-term behavior of the system after it has reached its maximum intensity. The conclusions are summarized in section 5.

2. NUMERICAL MODEL

The numerical model used in this study is a modified version of the axisymmetric tropical cyclone model of Rotunno and Emanuel (1987), which was used to simulate polar low development by Emanuel and Rotunno (1989). The nonhydrostatic, compressible equations of motion are integrated, using prognostic equations for momentum, potential temperature, nondimensional pressure, and mass mixing ratios of water vapour and ice. The turbulence parameterization is a first-order closure with a Richardson Number-dependent eddy viscosity. Changes for the present study include new parameterizations for radiation and cloud microphysics, as well as modifications to the boundary conditions. Otherwise, the configuration is the same that used by Emanuel and Rotunno (1989).

The simulations were initialized using the 12 GMT 13 December, 1982 thermodynamic sounding from Bear Island in the Norwegian Sea (Fig. 1). As described by Rasmussen (1985), an intense polar low was situated nearby at this time. To provide a better representation of the lowest levels of the troposphere at the polar low centre, the temperature and dewpoint temperature were increased below 830 mb, as described by Emanuel and Rotunno (1989) (their "warm, moist" case). As shown in Fig. 1, the relatively cool boundary layer is capped by a strong inversion between 830 and 950 mb. Above

this, the vertical stability of the troposphere is very weak.

An initial azimuthal wind field was prescribed in the form of a vortex with a maximum wind speed of 10 ms^{-1} at the surface at a radius of 50 km. The initial wind decreases linearly with height, with the functional form give by equation (15) of Emanuel and Rotunno (1989). The corresponding pressure and temperature distributions were found by integrating outwards from the axis of the vortex, assuming hydrostatic and gradient wind balance.

All of the model runs described in the following sections were carried out using a uniform grid spacing of 1 km in the vertical and 10 km in the radial direction, with a 20 s timestep. One of the runs was repeated twice, first with a horizontal grid size of 5 km, then with a vertical grid size of 500 m. In each case, the growth rate and structure of the polar low were not significantly changed, although the individual convective updrafts became narrower, with larger vertical velocities, when the horizontal resolution was increased.

(a) Domain size and boundary conditions

At the model's lower boundary, a constant sea surface temperature of 279 K was imposed. The surface drag and fluxes of latent and sensible heat were parameterized using bulk aerodynamic formulae, with a wind speed-dependent drag coefficient. The formulation differs from that given by Rotunno and Emanuel (1987) in that a minimum wind speed of 1 ms^{-1} was imposed in the heat and moisture flux calculations. For example, the surface flux of sensible heat was given by

$$F_z^\theta = C_E \max(|\mathbf{u}_1|, 1 \text{ ms}^{-1}) (\theta_{\text{surf}} - \theta_1),$$

where $C_E = 1.1 \times 10^{-3} + 4 \times 10^{-5} |\mathbf{u}_1|$, and $|\mathbf{u}_1|$ and θ_1 are velocity and temperature at the lowest model level. Fluxes of other quantities are calculated similarly. This ‘‘gust factor’’ can be thought of as representing the effects of turbulent gusts of wind in the boundary layer, on scales too small to be resolved (*cf.* Miller et al. 1992). In the polar low simulations, its inclusion served to prevent an artificial delay in the onset of convection, caused by a lack of surface fluxes in the outer part of the domain where the initial wind speed was small.

At the upper boundary, the absorbing layer used by Emanuel and Rotunno (1989) was retained. However, the top of the domain was moved to 18 km and the depth of the absorber was increased to 4 km to provide better absorption of vertically propagating gravity waves late in the simulations, when the tropopause height had increased.

The outer boundary was represented by a no-flux condition. To prevent reflection of gravity waves, an absorbing layer similar to that used at the top boundary, but with a thickness of 300 km, was employed. The radiation condition used by Emanuel and Rotunno was found to be inappropriate for long-term simulations since convection can develop near the boundary creating highly nonlinear flows. In testing, it was found that large mass flows across the boundary could occur, producing large-amplitude inertial oscillations. The location of the outer boundary was determined by increasing the size of the domain until the results became independent of its position. A domain size of 2500 km was found to be sufficient and was used for all the results presented in this paper. The reasons for this surprisingly large value are discussed in section 4.

(b) Radiation and microphysics

Only longwave radiation has been included in this study. The omission of shortwave solar heating was motivated in part by the life cycle of the Bear Island polar low, from which the initial sounding was taken. This system formed north of the Arctic Circle in winter and was never exposed to sunlight. The parameterization for longwave radiation was adapted from the UK Meteorological Office mesoscale model, and is based on the five band scheme of Roach and Slingo (1979). The emissivity of clouds is calculated using the model's predicted water content and, as in the operational mesoscale model, the difference in optical properties between water and ice is accounted for by scaling the absorber path length by a constant factor of 0.35.

The parameterization of cloud microphysics is described by Craig and Clough (1993), and will be summarized briefly here. All condensed water is assumed to be frozen, and a single variable is used for the mixing ratio of ice. Ice is assumed to fall with a terminal velocity, V_T , derived from the observations of Heymsfeld (1977), and given in metres per second by $V_T = 3.2(\rho q_i)^{0.17}(\rho_o/\rho)^{1/2}$, where q_i is the mixing ratio of ice, ρ is density and ρ_o is a reference density. This relationship is appropriate for small ice crystals, snow, and aggregates, but dense ice such as graupel and hail is ignored. In conditions of subsaturation with respect to ice, evaporation is assumed to occur instantly, until all ice is evaporated or saturation is restored. This assumption is justified by the calculations of Clough and Franks (1991), which showed that ice will typically fall only a few hundred metres in subsaturated conditions before evaporation, which is less than the vertical grid spacing in the present model. This is in contrast to raindrops, with higher terminal velocity and smaller surface area to mass ratios, which fall much fur-

ther before evaporation. It is also assumed that condensation occurs instantly to remove any supersaturation with respect to ice. This is probably the most questionable assumption of the microphysical parameterization, since the removal of supersaturation with respect to ice at temperatures above -40°C requires the presence of an adequate supply of freezing nuclei. However, this is not improbable in long-lived convective systems such as polar lows, where the remnants of previous clouds provide a source of small ice crystals. The situation is likely to be comparable to tropical cyclones, where observations show little liquid water at temperatures only a few degrees below freezing (Black and Hallet, 1986). An experiment illustrating the sensitivity of the results to this assumption is described at the end of the next section.

3. THE EFFECT OF RADIATION ON POLAR LOW INTENSIFICATION

The evolution of the maximum tangential wind speed in the simulated polar low is shown in Fig. 2, along with results for some experiments with modified physics which will be discussed below. For the first 10-15 hours of the simulation, prior to the outbreak of convection, the initial vortex weakens due to surface friction. From 15 to 60 hours, the polar low rapidly intensifies, reaching a maximum strength of about 45 ms^{-1} . After this time the system gradually decays. The rate of intensification of wind speed shown in Fig. 2, and corresponding average rate of decrease of surface pressure of 0.7 mb hr^{-1} , are not unreasonable for polar lows (cf. Rasmussen 1985), however the duration of the period of intensification, and the maximum wind speed and minimum central pressure (965 mb), are more extreme than are generally observed. Superimposed on the general increase in wind speed in Fig. 2 are rapid fluctuations with periods of 1-2 hours, associated with individual convective elements within the large-scale flow.

The structure of the polar low at 40 hours is shown in Fig. 3. During the period of rapid growth, the radius of maximum tangential wind is approximately 70 km (Fig. 3a). The vortex has a baroclinic structure, with winds decreasing to zero at the tropopause at 7 km, in approximate thermal wind balance with a potential temperature anomaly of about +5 K (Fig. 3b). The distribution of ice shown in Fig. 3c indicates a clear eye at the centre of the vortex with a radius of 50 km. Also visible are large concentrations of ice associated with convective updrafts in the eyewall, with smaller mixing ratios in the cirrus outflow at upper levels, extending to a radius of about 250 km. This dimension is comparable to that of the cloud features observed on satellite images of polar lows (Rasmussen 1989,

Nordeng and Rasmussen 1992). An area of suppressed convection is found immediately outside the vortex due to subsidence of air that has flowed out from the system at upper levels. The region from 500 km to the edge of the outer absorbing layer at 2200 km is characterized at this time by shallower convection which appears to be uninfluenced by the polar low's circulation.

In addition to the control simulation, Fig. 2 shows the evolution of the maximum tangential wind for an experiment in which the radiative heating and cooling was set to zero. Convection starts about 5 hours earlier in this run, but the vortex grows more slowly, reaching a maximum intensity of 38 ms^{-1} after 65 hours of growth. A direct assessment of the magnitude of the radiative cooling rates in comparison with the other terms in the thermodynamic equation is given in Fig. 4. Fig. 4a shows the total contribution of advection, latent heating, and diffusion to the rate of change of potential temperature, averaged over a 10 hour period from 40 to 50 hours. While condensation produces average heating rates of up to 190 K day^{-1} in the updraft region, this is largely offset by adiabatic cooling, leaving a net heating of only about 5 K day^{-1} in the core region (radius 0-100 km). In the immediate environment (radius 100-500 km), subsidence produces a warming of $1\text{-}2 \text{ K day}^{-1}$. Radiative cooling, on the other hand, has a negligible effect in most of the troposphere between 50 and 200 km radius, with cooling of about 1 K day^{-1} outside this region. The growth of the polar low is due to a net heating of its warm core relative to the environment of $3\text{-}4 \text{ K day}^{-1}$. Radiation provides an additional cooling of the environment relative to the core region of approximately 1 K day^{-1} .

The distribution of radiative cooling is determined by the location of cloud. This is visible in Fig. 3c where the region with cooling greater than 1 K day^{-1} is shaded. In the clear sky of the subsidence region, substantial cooling is found throughout the depth of the troposphere. In cloud however, even relatively small concentrations of ice are sufficient to act as black body absorbers in the infrared part of the spectrum. There is thus little divergence of radiative flux in the interior of the polar low, and little radiative heating or cooling. Cooling occurs in a relatively thin layer at the cloud top, but as it is confined to this level it has little effect on the developing warm core.

The magnitude and distribution of radiative cooling suggests that the mechanism by which it intensifies the polar low is by cooling the environment relative to the system's warm core. As noted in the introduction, it is also possible that enhancement of the growth rate is due to an overall destabilization of the atmosphere, without requiring the cooling to be localized away from the core. To distinguish between the two possibilities, a further experiment was carried out, in which the radiative cooling rates were calculated normally but then averaged in the horizontal before being added to the thermodynamic

equation at each timestep. Fig. 2 shows that when the cooling is averaged, the growth rate is substantially reduced, but still greater than when radiation was omitted entirely, particularly during the period from 60-75 hours. A further confirmation of the importance of the horizontal distribution is provided by the final experiment plotted in Fig. 2. In this simulation, the radiative parameterization was replaced by a simple Newtonian cooling, which relaxes the potential temperature field towards the initial state with a time scale of 1 day. While the domain-averaged cooling (not shown) is similar in magnitude to that obtained from the full radiation scheme, the maximum cooling rates are found at the centre of the warm core. Little cooling occurs in the environment where the temperature perturbation is smaller. This is directly opposite to the distribution produced by the full radiative parameterization, with the result that the vortex is damped to the point where no significant increase in wind speed occurs.

The importance of cloud in determining the distribution of radiative cooling suggests that the results may be rather sensitive to the parameterization of cloud microphysics. As discussed in section 2, the most questionable assumption in the present scheme is likely to be the instant removal of supersaturation with respect to ice, which wouldn't necessarily occur unless temperatures were well below 0 °C. As an example of the opposite extreme, the simulation was repeated with saturation calculated with respect to water. At the temperatures found in the midtroposphere in the present simulation, the saturation mixing ratio over water is up to 50% greater than over ice. Fig. 5 shows the growth rate in this case to be somewhat slower, but still much greater than when radiation was removed. The dependence of growth rate on the interaction of cloud and radiation field is thus modified quantitatively, but not qualitatively. Several factors appear to contribute to this difference, including delayed formation of cloud in the polar low environment, resulting in reduced mid-level cooling, and the reduction in latent heating due to reduced condensation. The simulation was also repeated using the parameterization of Golding (1993), which includes cloud water and rain as well as ice. The results (not shown) were between the two extremes described above. An experiment using the microphysical scheme of Emanuel and Rotunno (1989) will be discussed briefly in the next section.

The final curve in Fig. 5 shows the results of a run in which the ice was treated as water in the radiative parameterization. This modification had little effect on the growth of the polar low, but produced a slightly weaker vortex in the decaying phase. This was due to the optically denser clouds allowing slightly less radiative cooling, resulting in correspondingly weaker convection.

4. LONG-TERM BEHAVIOR

(a) Convection in the environment

When the simulation is continued for a sufficiently long period, the model atmosphere approaches a state of radiative-convective equilibrium, where heating at the surface is balanced by radiative cooling to space. A plot of the average tropospheric temperature perturbation in a region well away from the polar low vortex shows this progression (Fig. 6). The region cools by radiation for an initial period of 80 hours, until deep convection begins to mix heat through the troposphere. The atmosphere then warms until equilibrium is reached after about 300 hours.

Fig. 6 also shows the evolution of average temperature for a simulation using the microphysical parameterization of Emanuel and Rotunno (1989). In their scheme, rather than calculating the fall speed of ice as a continuous function of mixing ratio, any amount up to 1 g kg^{-1} is considered to be cloud ice with zero terminal velocity, while any excess over this amount is assumed to fall with speed 1 ms^{-1} . When this parameterization was used, the atmospheric temperature continued to rise, with no indication of approaching an equilibrium state, until the simulation was terminated due to numerical instability. As shown by Craig and Clough (1993), the middle and upper troposphere rapidly filled with ice detrained from cumulus updrafts, since only the excess over 1 g kg^{-1} could fall out. As a result, radiative cooling was completely blocked, except at the cloud top. A similar accumulation of cloud has been reported in long-term simulations using the Kessler warm rain parameterization (Islam 1991).

The convection in the equilibrium state shows considerable organization (Fig. 7). Initially, there is strong conditional instability and convective cells are closely spaced, although some tendency for clustering is visible. As the atmosphere equilibrates, weaker clusters are suppressed by subsidence from their stronger neighbours. After about 180 hours, the convective activity consists of five clusters, in addition to the polar low. This behavior is similar to that obtained in previous simulations of two-dimensional convection (eg. Asai and Nakasuji 1977, 1982), and is consistent with the weakly nonlinear theory of Bretherton (1987, 1988). According to Bretherton's theory, the spacing of the clusters is set by the extent of the subsidence region, which is determined by the lesser of the Rossby radius of deformation and a length scale for diffusive dissipation of internal gravity waves. Experiments with different values of the Coriolis parameter (not shown) show that in the present case the spacing of the clusters depends linearly on the rotation rate. For the case shown in Fig. 7, a rough estimate of the

radius of deformation in the equilibrium state is given by $NH/f = 360$ km, where the Brunt-Vaisala frequency is $N = 7 \times 10^{-3} \text{ s}^{-1}$, the depth of the troposphere is $H = 7$ km, and the Coriolis parameter is $f = 1.36 \times 10^{-4} \text{ s}^{-1}$. This distance is approximately equal to the spacing of the cloud clusters.

The need to accommodate an ensemble of widely-spaced convective clusters is the reason that the size of the domain must be so much larger than the polar low itself. As shown by Bretherton (1988), a small domain can result in the subsidence from a cluster being forced to occur in an unnaturally small region, leading to spurious intermittency as clouds are alternately suppressed and allowed to develop. On a sufficiently large domain, the adjustments required to accommodate a number of quasi-permanent clusters will be small regardless of any changes in the domain size. It is important to note that the organization seen in this simulation is a two-dimensional effect. In three dimensions the area of subsidence around a cloud cluster is proportional to the square of the distance from the updraft, and the effects of compensating subsidence have a shorter range.

(b) The polar low

The polar low grows rapidly from 15 to 60 hours of the simulation. This is seen the plot of maximum azimuthal wind speed in Fig. 2, and in the time-radius section of low-level wind in Fig. 8a. After 60 hours the region of high winds broadens, while the maximum moves towards larger radius and weakens. These changes are accompanied by changes in the thermal structure of the system. Fig. 8b shows that the mid-level potential temperature in the core region (radius less than 100 km) increases rapidly from 15 to 60 hours. This produces a large radial temperature gradient between the core and the region outside, which warms more slowly. The intensification of the temperature gradient is accompanied by the intensification of the azimuthal wind, as expected from thermal wind balance. While the core temperature continues to increase until about 120 hours, the rate of increase is slower than that of the surrounding air. As a result, the radial temperature gradient is reduced and the azimuthal wind speed begins to decrease.

The maximum value of potential temperature reached in the core region is about 302 K. This is the potential temperature of an air parcel that has undergone saturated ascent from the sea surface temperature of 279 K (Fig. 1), and thus represents the maximum temperature that air in the simulated polar low could be expected to attain. The region outside the core ceases to warm at about 150 hours. Equilibrium here is reached earlier than in regions well away from the polar low (Fig. 6) due to larger sur-

face fluxes of heat and moisture in the vortex, associated with larger surface wind speeds.

The temperature gradient between the maximum value in the core and the radiative-convective equilibrium temperature at larger radius could, in principle, maintain a fairly intense, steady-state cyclone, consistent with the Carnot cycle model of Emanuel (1986). For the simulated polar low, this does not occur. As the radius of maximum wind moves outwards, the structure of the vortex undergoes a transition to the form illustrated in Fig. 9. An upper-level wind maximum spins up in the centre of the system, while the low-level vortex decays. As shown by Emanuel and Rotunno (1989), this structure is obtained when the maximum heating, which occurs in the eyewall just inside the radius of maximum winds, is located at a radius large compared to the radius of deformation. A diagnostic calculation of the secondary circulation induced by a ring of heating in a balanced vortex showed that if the heating was placed inside the radius of deformation, the result was strongly constrained by the circular geometry. The secondary circulation was induced predominantly to the outside of the heating ring, producing inflow and spinup of the cyclone at low levels. Because of the small radius of deformation associated with the large value of the Coriolis parameter in polar regions, this situation only occurs early in the simulation, before the tropospheric temperatures rise and the warm core expands. Eventually the heating moves to larger radius, allowing the outflow from the heating region to have a substantial component in towards the axis, producing the upper-level spinup seen in Fig. 9. In addition, as the radius of heating expands, the effective radius of deformation decreases due to the increasing vorticity of the polar low. This effect is discussed further by Schubert and Hack (1982), van Delden (1989), and in the appendix of Craig and Cho (1992a). In an additional experiment (not shown), the value of the Coriolis parameter was reduced by a factor of 10 at 240 hours of the simulation. The resulting radius of deformation was much larger than the size of the polar low vortex, with the consequence that the transition in structure was immediately reversed and the low level winds reintensified.

The details of the decay after the transition in structure are not likely to be of relevance to polar lows in the atmosphere, since the expansion of the eyewall to a radius larger than the radius of deformation implies a weakening of the axisymmetric constraint. The vortex would then be vulnerable to three-dimensional instabilities or deformation by environmental flows.

A steady state polar low was not obtained in any of the simulations described here, but it is conceivable that the intensity of the vortex is still limited by the maximum values given by the Carnot cycle model. Emanuel and Rotunno (1989) gave a prediction for the minimum central pressure of the polar low which formed in the environment used to initialize the present simulations. The value they

obtained (922 mb) corresponded to a much more intense system than occurred in either the observations or in the simulations. However, the observed low-level temperature and moisture content in the atmosphere were considerably smaller than at the sea surface. Using these values to define the temperature of the warm reservoir in the Carnot cycle calculation, reasonable agreement was obtained with the observed central pressure. An analogous calculation was performed for the present simulation at the time of maximum intensity (60 hrs), using the lowest model level temperature and moisture content at the eyewall radius (65 km), and an environmental sounding obtained by averaging in radius between 500 and 2200 km. This reproduced the minimum central pressure of 967 mb to within 1 mb. While encouraging, the degree of the agreement is probably fortuitous, and is sensitive to choice of eyewall radius versus central temperature and moisture, and to the definition of the environmental sounding. These considerations will be explored more fully in future work.

5. CONCLUSIONS

The principal result of this investigation is that longwave radiative cooling can provide a significant enhancement to the growth of a simulated, axisymmetric, convective polar low. The main mechanism for this enhancement is cooling of the regions surrounding the warm core of the polar low, enhancing the radial temperature gradient produced by release of latent heat. The convective destabilization produced by mean cooling of the troposphere played a lesser role. This latter result is in contrast to the finding of Dudhia (1989) that cloud/clear-air cooling rate differences had little effect on a simulated tropical mesoscale convective system. The difference is presumably that the intensity of that system was not dependent on thermal wind balance with a warm core. These findings suggest that the effects of radiation found in simulations here may be present in any polar low with a warm core, including those where baroclinic instability or other processes also play a role in the development.

The organization of radiative cooling in such a way as to enhance polar low growth is due to the distribution of cloud, and is thus sensitive to both the microphysical parameterization, and to the treatment of cloud optical properties in the radiation scheme. There is great uncertainty in both these areas, but both are the subject of considerable research at present.

The second main result of this work is the failure to produce a steady-state cyclone as envisaged in the Carnot cycle model. The maximum intensity of the polar low was not maintained since the environment continued to warm for some time after the core region reached its maximum temperature.

Even when the environment reached equilibrium, the vortex continued to decay due to a change in structure to a predominantly upper-level system. This change occurred because the radius of deformation in polar regions is comparable to the size of the system. These results suggest that polar lows may be a transitory part of the air mass transition in a cold air outbreak, with a finite lifetime even in the absence of changes in external forcing, such as happens when the system makes landfall.

Preliminary calculations do indicate however, that at the time of maximum intensity, the polar low may be in a quasi-equilibrium configuration, as described by the Carnot cycle model, even though the boundary layer equivalent potential temperature does not closely approach the sea surface value and a steady state is not maintained. Furthermore, the apparent lack of a steady state in the present simulations may not be directly relevant to tropical cyclones. The radius of deformation in the tropics is always much larger than the cyclone scale, implying that the transition to an upper-level vortex structure would not occur. Secondly the tropical atmosphere is much closer to radiative-convective equilibrium than the rapidly-changing air mass in a cold air outbreak, and could thus provide a steady-state environment which could maintain the cyclone close to its maximum intensity.

ACKNOWLEDGEMENTS

The author would like thank Richard Rotunno for providing the axisymmetric model code, Sue Ballard for providing the radiative transfer scheme, and Sid Clough and Brian Golding for assistance with the cloud microphysical parameterizations. This work has also benefited substantially from discussions with Alan Thorpe, Tim Hewson, Kerry Emanuel, Craig Bishop, and Virginie Marecal. Finally, I would like to thank Suzanne Gray, who performed the Carnot cycle calculations described in section 4.

REFERENCES

- Black, R. A., and J. Hallet, 1986: Observations of the distribution of ice in hurricanes. *J. Atmos. Sci.*, 43, 802-822.
- Bretherton, C. S., 1987: A theory for nonprecipitating moist convection between two parallel plates. Part I: Thermodynamics and "linear" solutions. *J. Atmos. Sci.*, 44, 1809-1827.
- Bretherton, C. S., 1988: A theory for nonprecipitating moist convection between two parallel plates.

- Part II: Nonlinear theory and cloud field organization. *J. Atmos. Sci.*, 45, 2391-2415.
- Asai, T., and I. Nakasuji, 1977: On the preferred mode of cumulus convection in a conditionally unstable atmosphere. *J. Meteor. Soc. Japan*, 55, 151-167.
- Asai, T., and I. Nakasuji, 1982: A further study of the preferred mode of cumulus convection in a conditionally unstable atmosphere. *J. Meteor. Soc. Japan*, 60, 425-430.
- Businger, S., and R. J. Reed, 1989: Cyclogenesis in cold air masses. *Weather and Forecasting*, 4, 133-156.
- Businger, S., and J.-J. Baik, 1991: An arctic hurricane over the Bering Sea. *Mon. Wea. Rev.*, 119, 2293-2322.
- Businger, S., and B. Walter, 1988: Comma cloud development and associated rapid cyclogenesis over the Gulf of Alaska: A case study using aircraft and operational data. *Mon. Wea. Rev.*, 116, 1103-1123.
- Chen, S., and W. R. Cotton, 1988: The sensitivity of a simulated extratropical mesoscale convective system to longwave radiation and ice-phase microphysics. *J. Atmos. Sci.*, 45, 3897-3910.
- Clough, S. A., and R. A. A. Franks, 1991: The evaporation of frontal and other stratiform precipitation. *Quart. J. Roy. Meteor. Soc.*, 117, 1057-1080.
- Craig, G. C., and H.-R. Cho, 1988: Cumulus convection and CISK in the extratropical atmosphere. Part I: Polar lows and comma clouds. *J. Atmos. Sci.*, 45, 2622-2640.
- Craig, G. C., and H.-R. Cho, 1992a: Cumulus convection and CISK in the extratropical atmosphere. Part II: Comma-cloud formation in cyclonic shear regions. *J. Atmos. Sci.*, 49, 1318-1333.
- Craig, G. C., and H.-R. Cho, 1992b: A study of two cases of comma-cloud cyclogenesis using a semi-geostrophic model. *Mon. Wea. Rev.*, 120, 2942-2961.
- Craig, G. C., and S. A. Clough, 1993: A parameterization for ice-phase microphysics in mesoscale models. *Mesoscale Modelling Newsletter*, No. 4, Feb. 1993, available from Joint Centre for Mesoscale Meteorology, University of Reading, Reading, UK.
- Dudhia, J., 1989: Numerical study of convection observed during the Winter Monsoon Experiment using a mesoscale two-dimensional model. *J. Atmos. Sci.*, 46, 3077-3107.
- Emanuel, K. A., 1986: An air-sea interaction theory for tropical cyclones. Part I. *J. Atmos. Sci.*, 43, 585-604.
- Emanuel, K. A., and R. Rotunno, 1989: Polar lows as arctic hurricanes. *Tellus*, 41A, 1-17.
- Gray, W. M., and R. W. Jacobson, Jr., 1977: Diurnal variation of oceanic deep cumulus convection.

- Mon. Wea. Rev.*, 105, 1171-1188.
- Golding, B. W., 1993: A numerical investigation of tropical island thunderstorms. *Mon. Wea. Rev.*, 121, 1417-1433.
- Hack, J. J., 1980: The role of convective-scale processes in tropical cyclone development. PhD thesis, Colorado State University.
- Harold, T. W., and K. A. Browning, 1969: The polar low as a baroclinic disturbance. *Quart. J. Roy. Meteor. Soc.*, 95, 710-723.
- Heymsfeld, A. J., 1977: Precipitation development in stratiform ice clouds: A microphysical and dynamical study. *J. Atmos. Sci.*, 35, 1070-1096.
- Islam, S., 1991: *Predictability of mesoscale precipitation*. PhD thesis, Massachusetts Institute of Technology.
- Kurihara, Y., and R. E. Tuleya, 1981: A numerical simulation study on the genesis of a tropical storm. *Mon. Wea. Rev.*, 109, 1629-1653.
- Lystad, M., Ed., 1986: Polar lows in the Norwegian, Greenland and Barents Seas. Final Report, Polar Lows Project. The Norwegian Meteorological Institute, Oslo, Norway, 196 pp.
- Miller, M. J., A. C. M. Beljaars, and T. N. Palmer, 1992: The sensitivity of the ECMWF model to the parameterization of evaporation from the tropical oceans. *J. Climate*, 5, 418-434.
- Miller, R. A., and W. M. Frank: 1993: Radiative forcing of simulated tropical cloud clusters. *Mon. Wea. Rev.*, 121, 482-498.
- Nordeng, T. E., and E. Rasmussen, 1992: A most beautiful polar low. A case study of a polar low development in the Bear Island region. *Tellus*, 44A, 81-99.
- Rasmussen, E., 1979: The polar low as an extratropical CISK disturbance. *Quart. J. Roy. Meteor. Soc.*, 105, 531-545.
- Rasmussen, E., 1985: A case study of a polar low development over the Barents Sea. *Tellus*, 37, 407-418.
- Rasmussen, E., 1989: A comparison study of tropical cyclones and polar lows. In *Polar and Arctic Lows*, P. F. Twitchell, E. Rasmussen, and K. L. Davidson, eds. A Deepak Publishing, Vi, USA, 47-80.
- Reed, R. J., 1979: Cyclogenesis in polar airstreams. *Mon. Wea. Rev.*, 107, 38-52.
- Roach, W. T., and A. Slingo, 1979: A high resolution infrared radiative transfer scheme to study the interaction of radiation with cloud. *Quart. J. Roy. Meteor. Soc.*, 105, 603-614.

- Rotunno, R., and K. A. Emanuel, 1987: An air-sea interaction theory for tropical cyclones. Part II. *J. Atmos. Sci.*, 44, 542-561.
- Schubert, W. H., and J. J. Hack, 1982: Inertial stability and tropical cyclone development. *J. Atmos. Sci.*, 39, 1687-1697.
- Tao, W.-K., J. Simpson, and S.-T. Soong, 1987: Statistical properties of a cloud ensemble: A numerical study. *J. Atmos. Sci.*, 44, 3175-3187.
- van Delden, A., 1989: On the deepening and filling of balanced cyclones by diabatic heating. *Meteorol. Atmos. Phys.*, 41, 127-145.

FIGURE CAPTIONS

Figure 1. Tephigram with plotted temperature (solid line) and dewpoint temperature (dashed line), used for initial conditions at zero radius. The dash-dotted line shows the moist adiabat corresponding to the sea surface temperature of 279 K.

Figure 2. Maximum azimuthal wind speed as a function of time for three simulations: control (thick solid line), no radiation (thin solid line), horizontally averaged radiative heating/cooling (dashed line), and with the radiation scheme replaced by Newtonian cooling (dotted line).

Figure 3. Radius-height sections for the control experiment, at 40 hours, of (a) azimuthal wind speed (contour interval 5 ms^{-1} , dashed lines indicate negative values), (b) potential temperature perturbation (contour interval 2 K), (c) mixing ratio of ice (contours at 1, 0.01, and 0.0001 g kg^{-1}). Shading in (c) indicates radiative cooling rates greater than 1 K day^{-1} .

Figure 4. Radius-height sections for the control experiment, averaged from 40 to 50 hours, of local rate of change of potential temperature due to (a) advection, diffusion, and release of latent heat (contour interval 4 K day^{-1}), and (b) longwave radiation (contour interval 2 K day^{-1}). The shading is the same in (a) and (b), with dark gray denoting heating rates less than -4 K day^{-1} , medium gray heating rates between -4 and 0 K day^{-1} , and light gray heating rates from 0 to 4 K day^{-1} .

Figure 5. Maximum azimuthal wind speed as a function of time for the control simulation (thick solid line), no radiation (thin solid line), and simulations with saturation vapour pressure calculated over water (dashed line), and with cloud optical properties as for water (dotted line).

Figure 6. Deviation of temperature from its initial value, averaged over the region from 1500 to 2000 km in radius, and 0 to 8 km in height, for the control simulation (solid line), and an experiment using the microphysical parameterization of Emanuel and Rotunno (1989) (dashed line).

Figure 7. Region where ice concentration is greater than or equal to $2 \times 10^{-4} \text{ g kg}^{-1}$ at model level 2 ($z = 1.5 \text{ km}$), plotted as a function of radius and time.

Figure 8. (a) Azimuthal velocity at model level 2 ($z = 1.5$ km) (contour interval 5 ms^{-1}), and (b) potential temperature at model level 4 ($z = 3.5$ km) (contour interval 2 K), plotted as functions of radius and time.

Figure 9. Radius-height section of azimuthal wind speed for the control experiment, at 180 hours (contour interval 5 ms^{-1} , dashed lines indicate negative values).

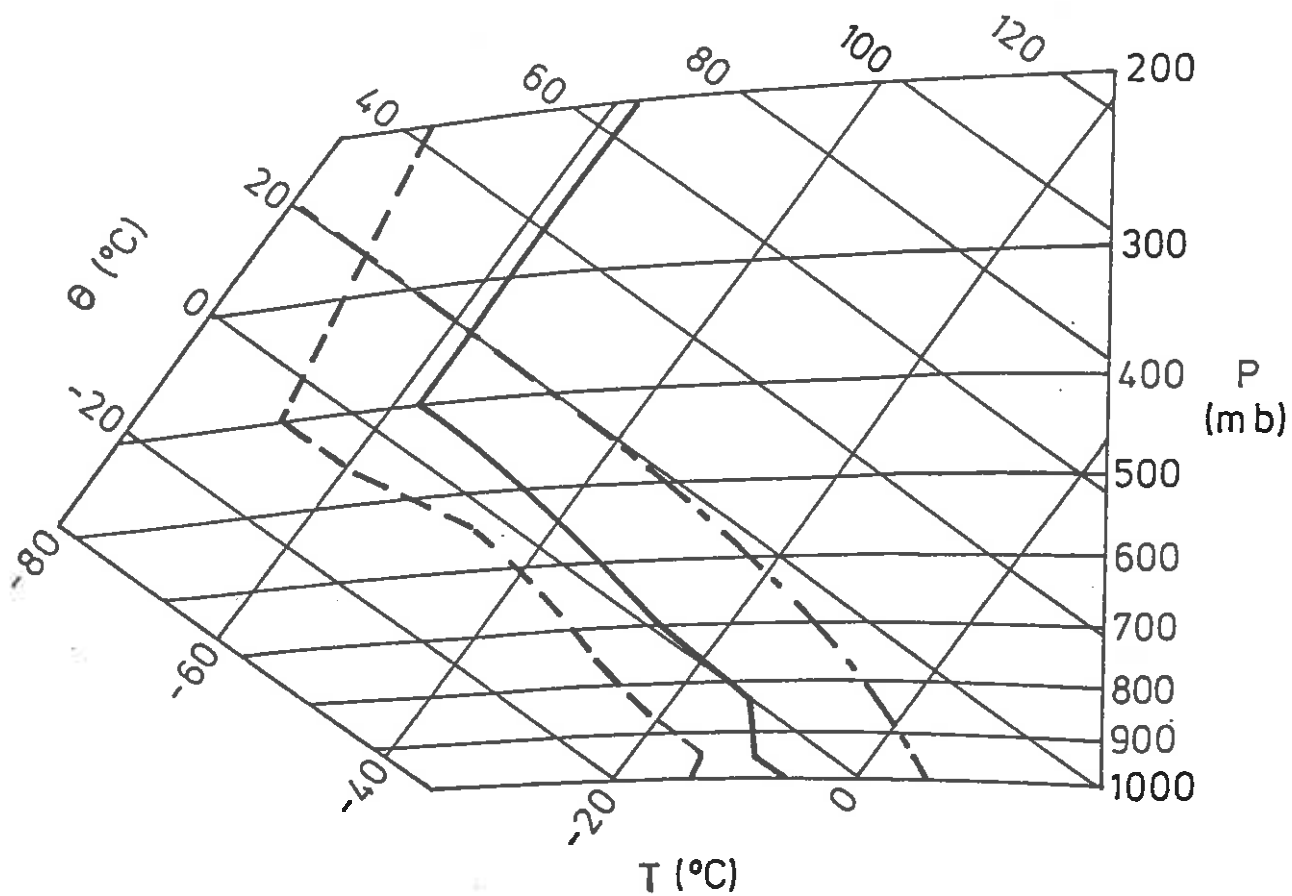


Figure 1. Tephigram with plotted temperature (solid line) and dewpoint temperature (dashed line), used for initial conditions at zero radius. The dash-dotted line shows the moist adiabat corresponding to the sea surface temperature of 279 K.

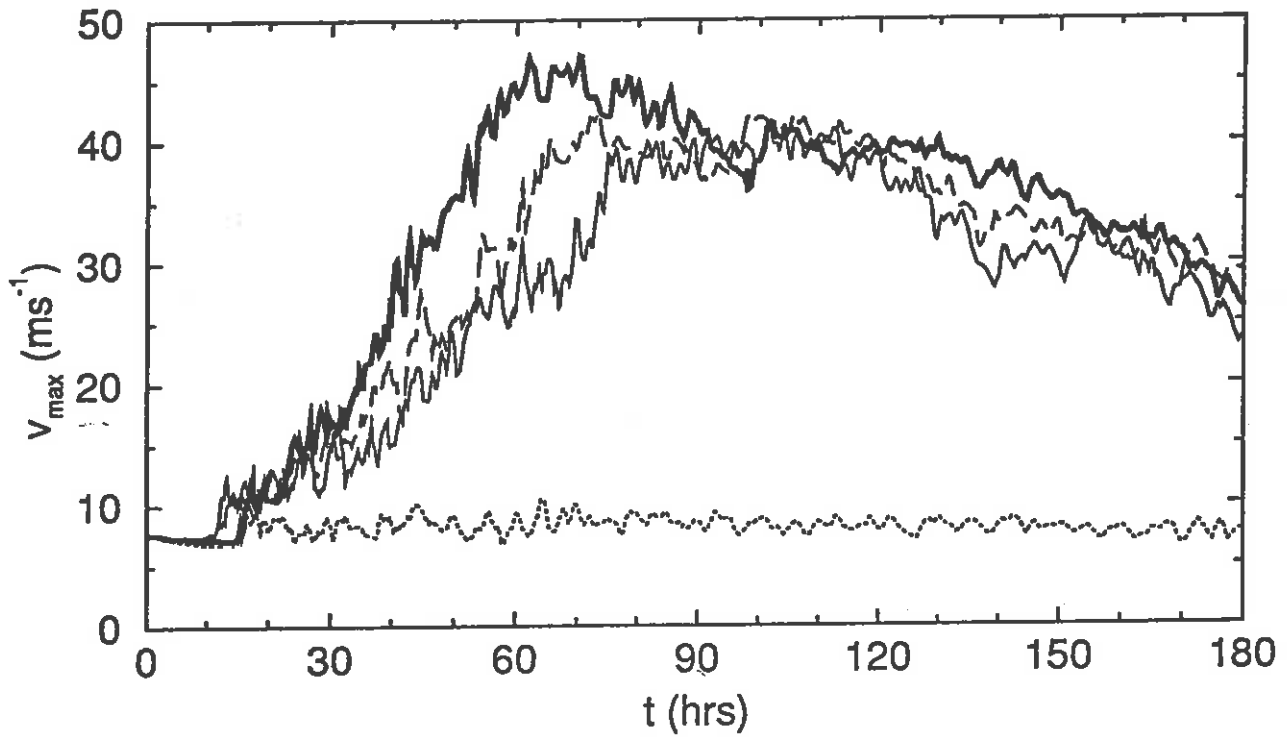


Figure 2. Maximum azimuthal wind speed as a function of time for three simulations: control (thick solid line), no radiation (thin solid line), horizontally averaged radiative heating/cooling (dashed line), and with the radiation scheme replaced by Newtonian cooling (dotted line).

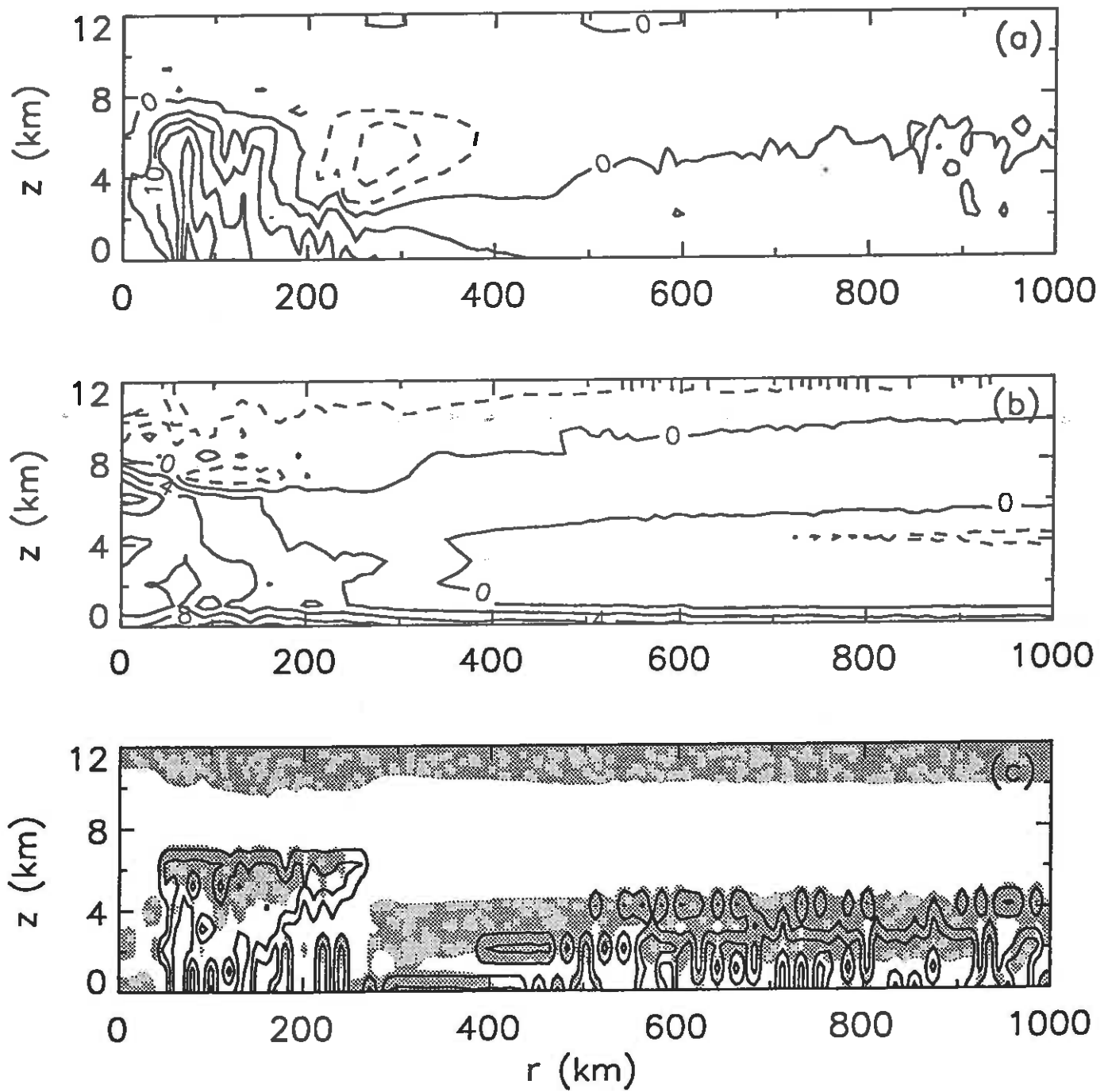


Figure 3. Radius-height sections for the control experiment, at 40 hours, of (a) azimuthal wind speed (contour interval 5 ms^{-1} , dashed lines indicate negative values), (b) potential temperature perturbation (contour interval 2 K), (c) mixing ratio of ice (contours at 1, 0.01, and 0.0001 g kg^{-1}). Shading in (c) indicates radiative cooling rates greater than 1 K day^{-1} .

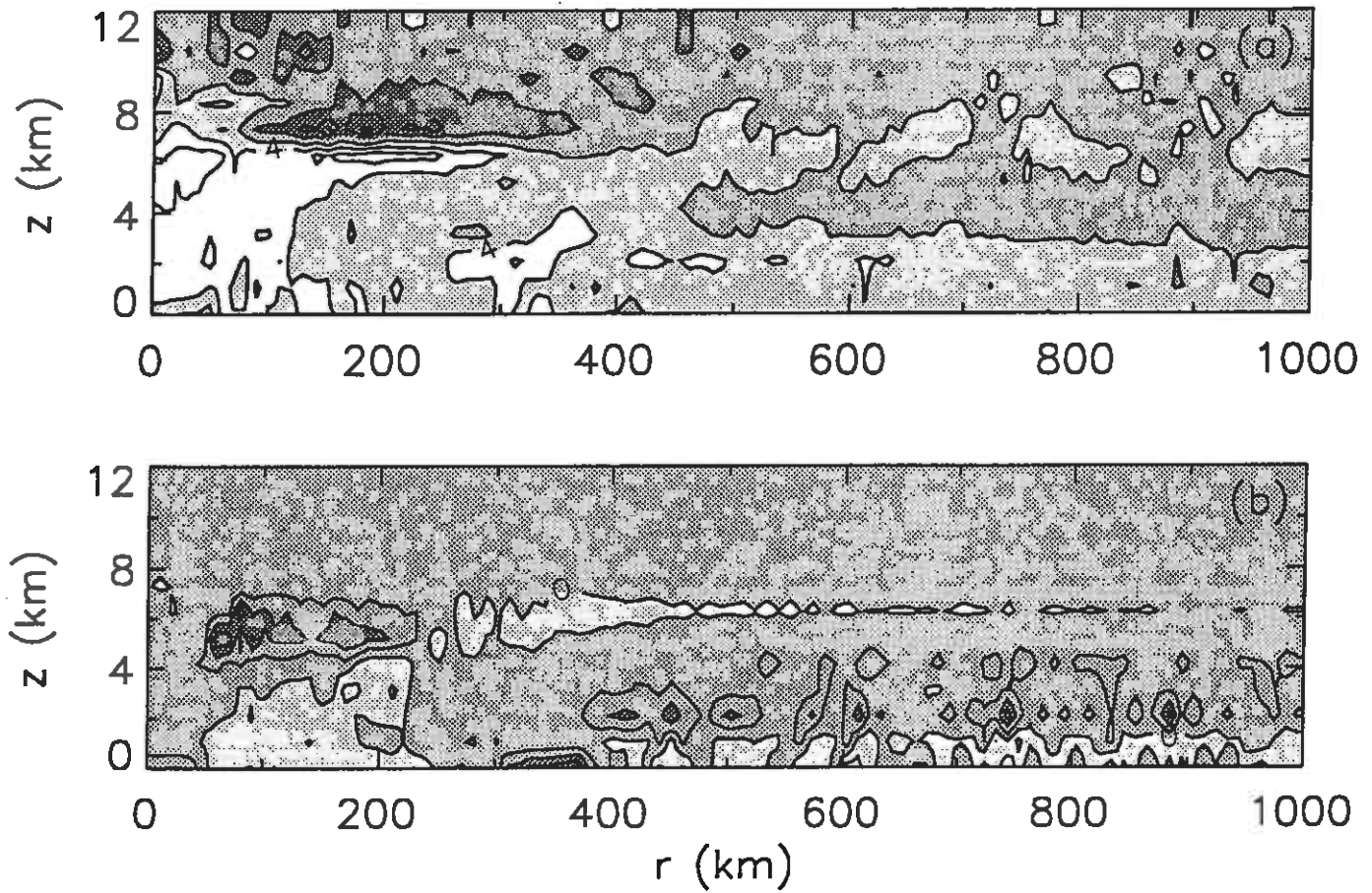


Figure 4. Radius-height sections for the control experiment, averaged from 40 to 50 hours, of local rate of change of potential temperature due to (a) advection, diffusion, and release of latent heat (contour interval 4 K day^{-1}), and (b) longwave radiation (contour interval 2 K day^{-1}). The shading is the same in (a) and (b), with dark gray denoting heating rates less than -4 K day^{-1} , medium gray heating rates between -4 and 0 K day^{-1} , and light gray heating rates from 0 to 4 K day^{-1} .

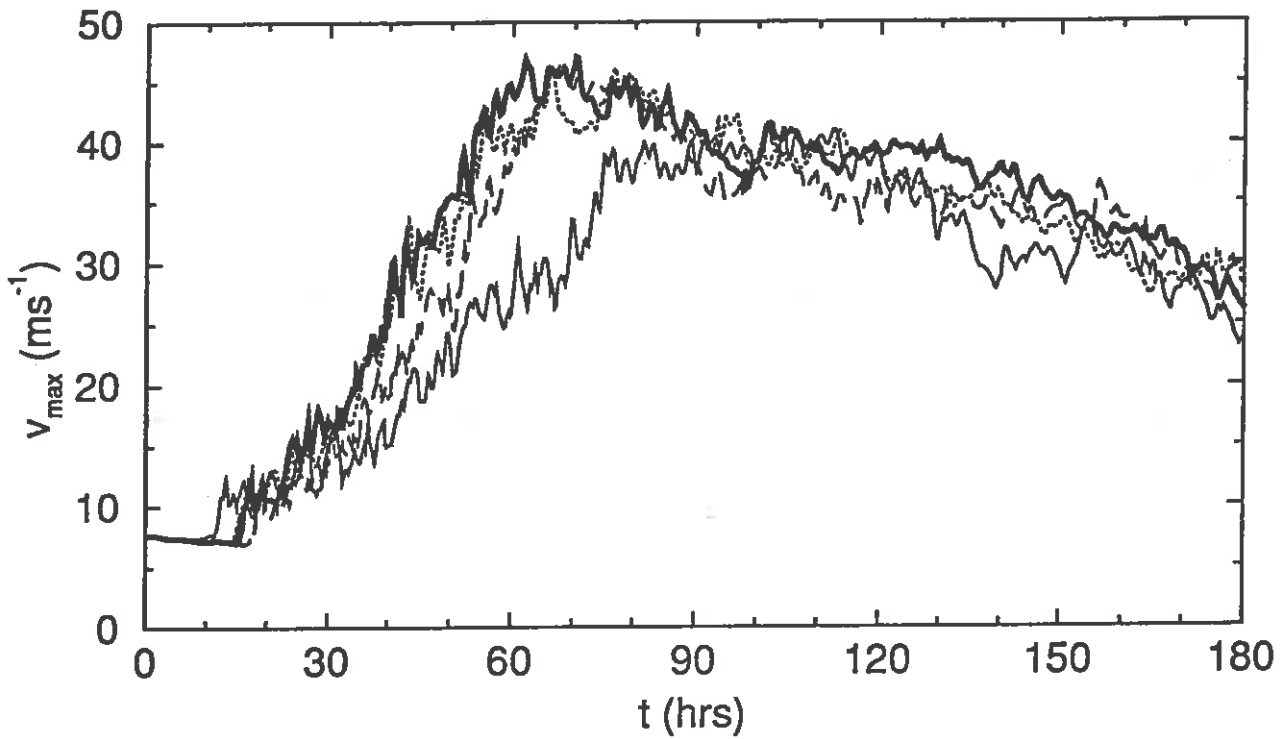


Figure 5. Maximum azimuthal wind speed as a function of time for the control simulation (thick solid line), no radiation (thin solid line), and simulations with saturation vapour pressure calculated over water (dashed line), and with cloud optical properties as for water (dotted line).

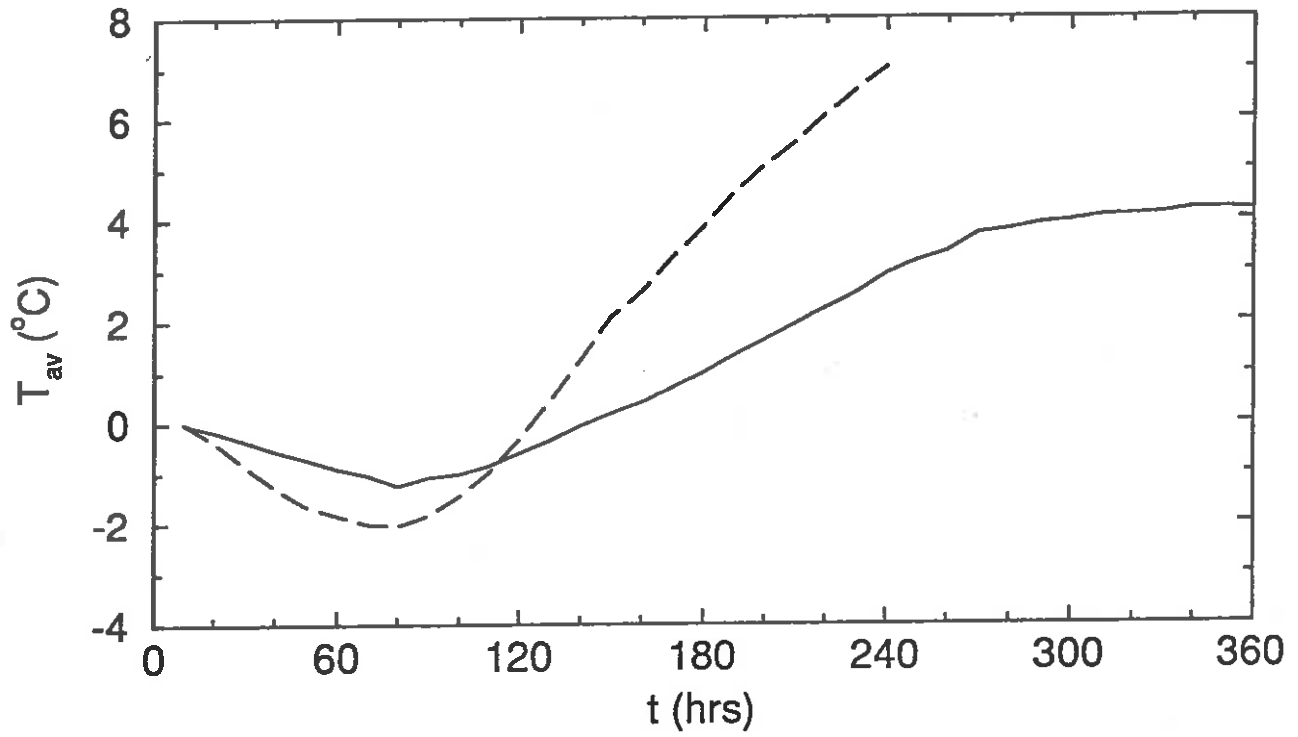


Figure 6. Deviation of temperature from its initial value, averaged over the region from 1500 to 2000 km in radius, and 0 to 8 km in height, for the control simulation (solid line), and an experiment using the microphysical parameterization of Emanuel and Rotunno (1989) (dashed line).

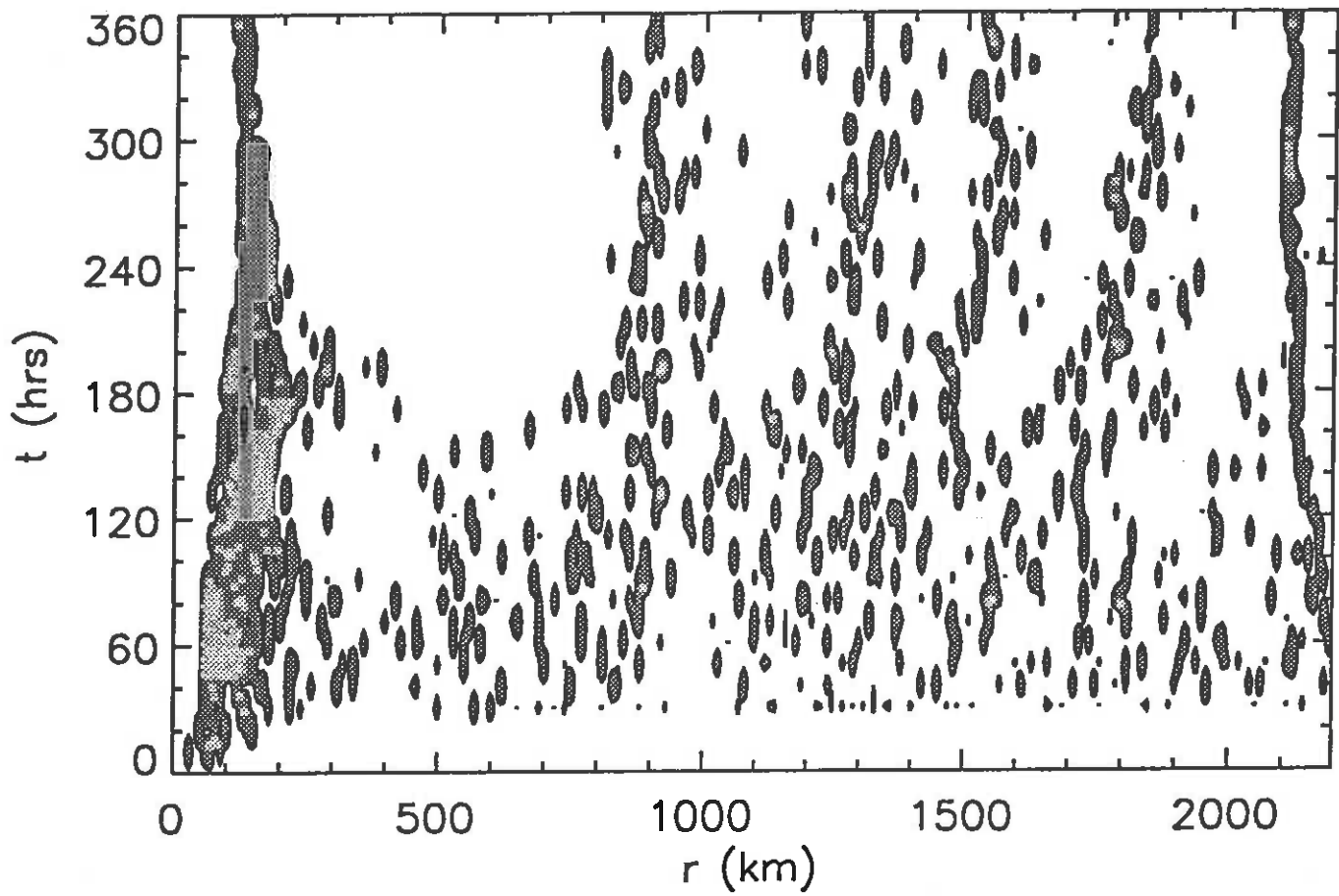


Figure 7. Region where ice concentration is greater than or equal to $2 \times 10^{-4} \text{ g kg}^{-1}$ at model level 2 ($z = 1.5 \text{ km}$), plotted as a function of radius and time.

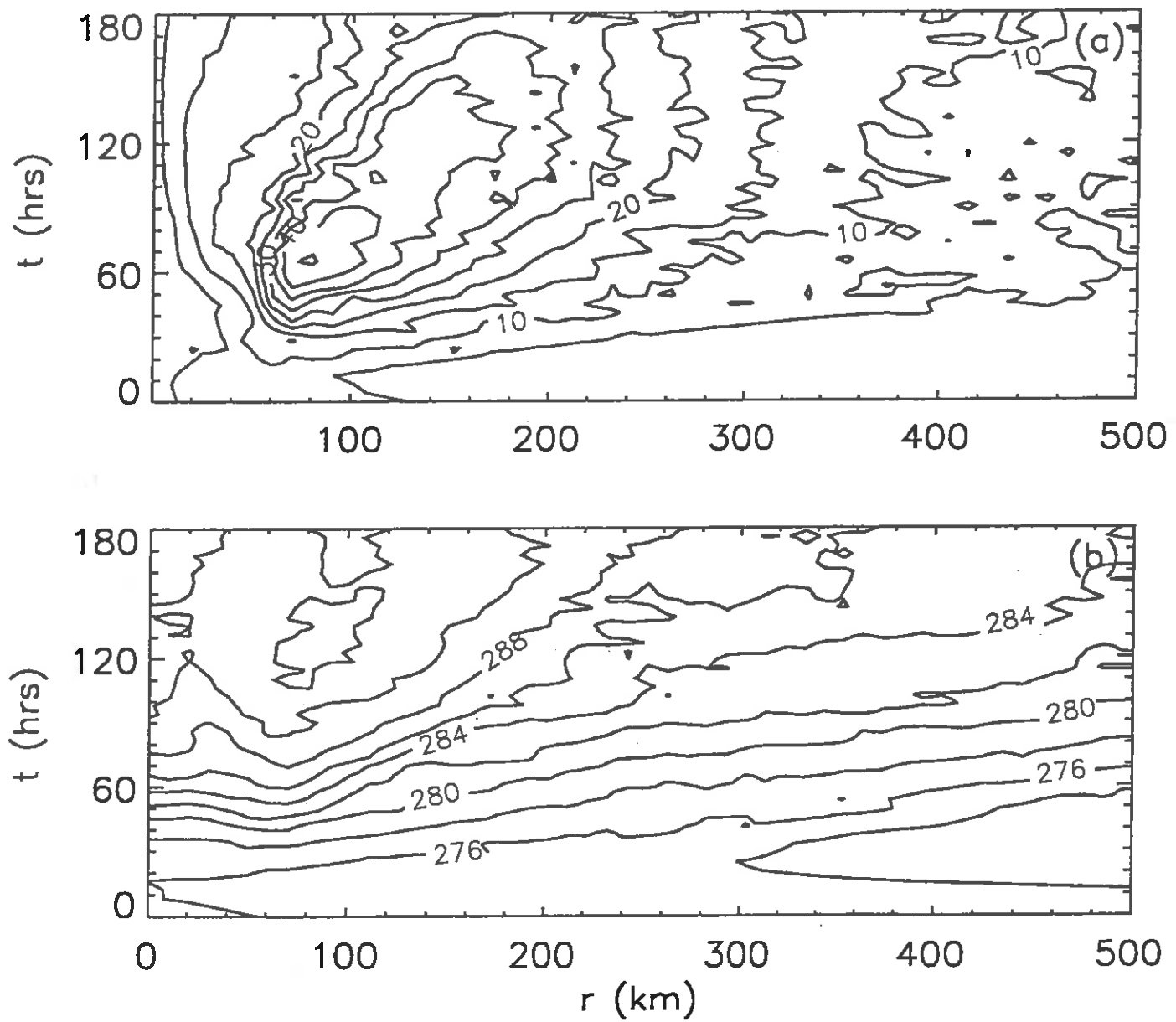


Figure 8. (a) Azimuthal velocity at model level 2 ($z = 1.5$ km) (contour interval 5 ms^{-1}), and (b) potential temperature at model level 4 ($z = 3.5$ km) (contour interval 2 K), plotted as functions of radius and time.

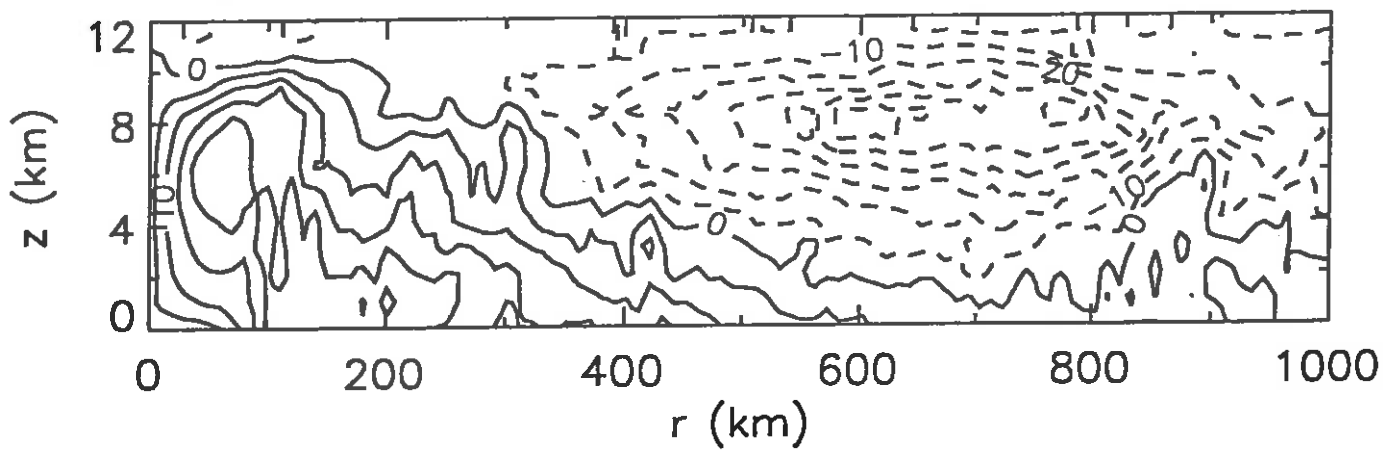


Figure 9. Radius-height section of azimuthal wind speed for the control experiment, at 40 hours (contour interval 5 ms^{-1} , dashed lines indicate negative values).

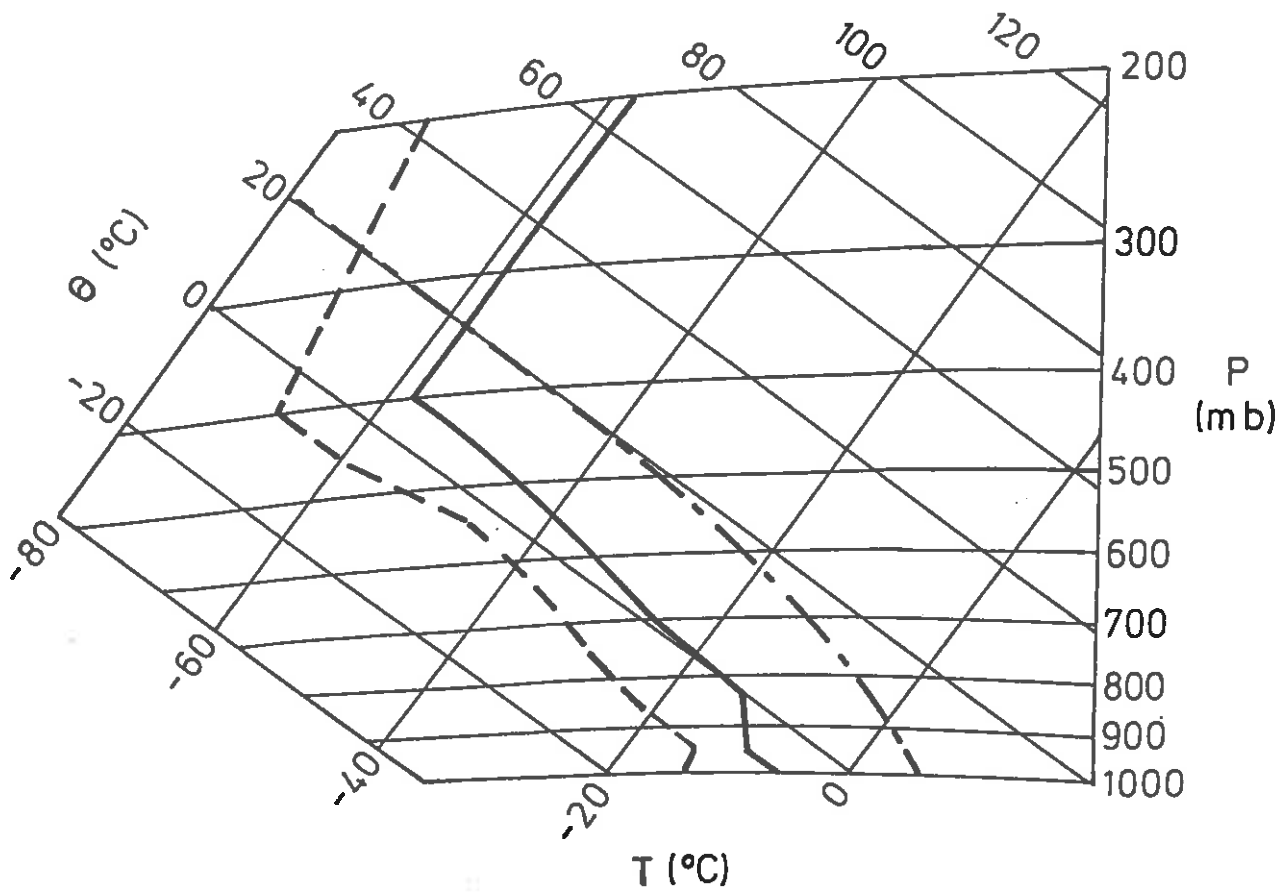


Figure 1. Tephigram with plotted temperature (solid line) and dewpoint temperature (dashed line), used for initial conditions at zero radius. The dash-dotted line shows the moist adiabat corresponding to the sea surface temperature of 279 K.

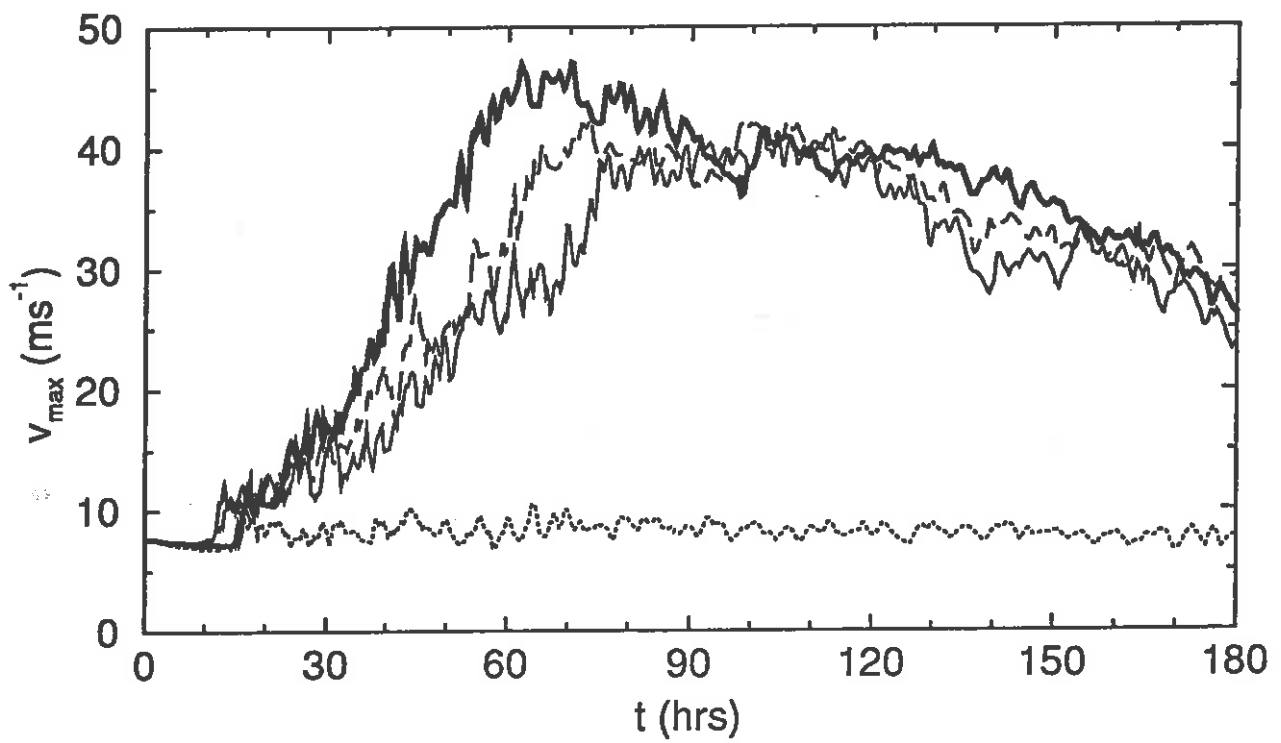


Figure 2. Maximum azimuthal wind speed as a function of time for three simulations: control (thick solid line), no radiation (thin solid line), horizontally averaged radiative heating/cooling (dashed line), and with the radiation scheme replaced by Newtonian cooling (dotted line).

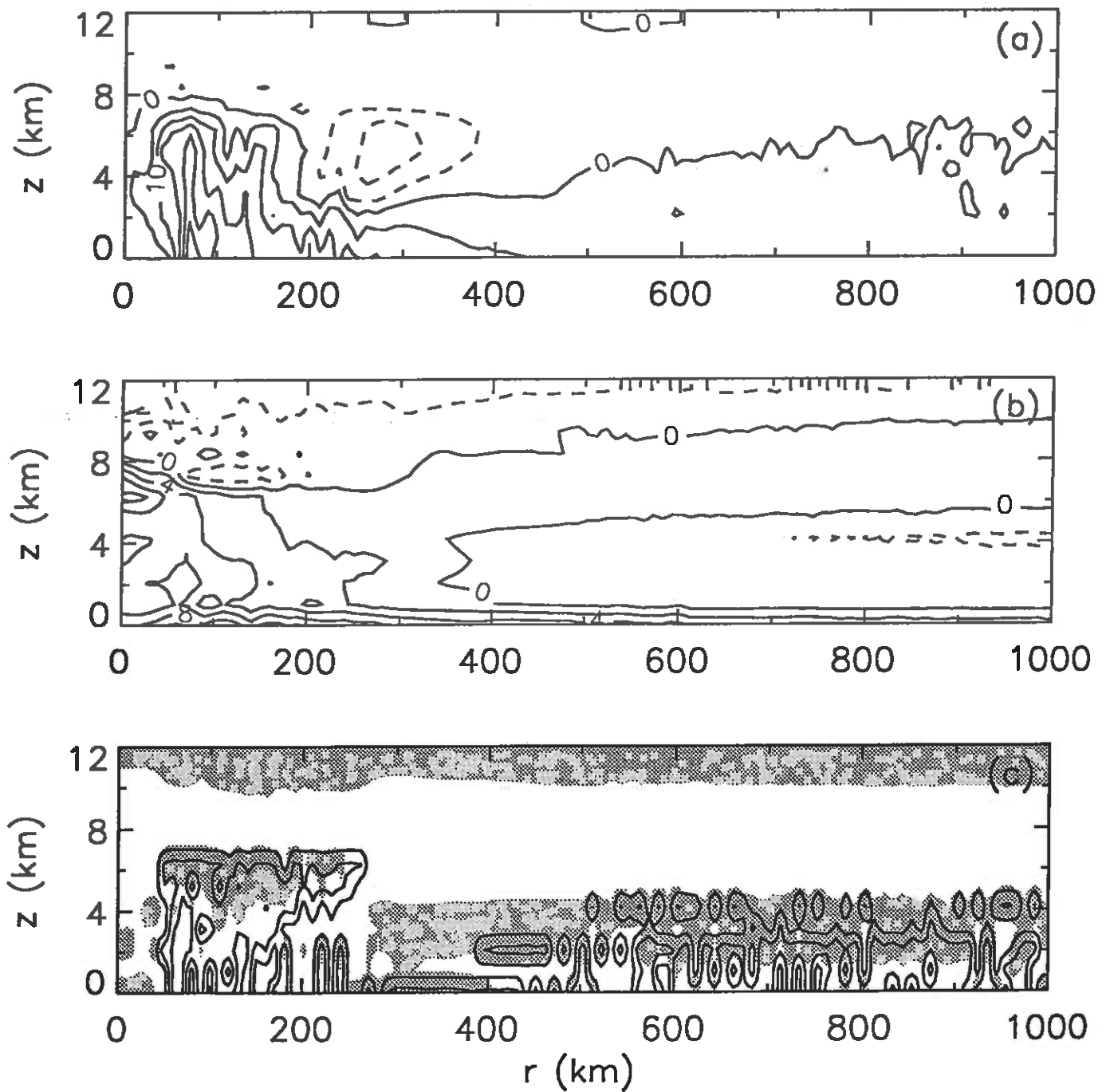


Figure 3. Radius-height sections for the control experiment, at 40 hours, of (a) azimuthal wind speed (contour interval 5 ms^{-1} , dashed lines indicate negative values), (b) potential temperature perturbation (contour interval 2 K), (c) mixing ratio of ice (contours at 1, 0.01, and 0.0001 g kg^{-1}). Shading in (c) indicates radiative cooling rates greater than 1 K day^{-1} .

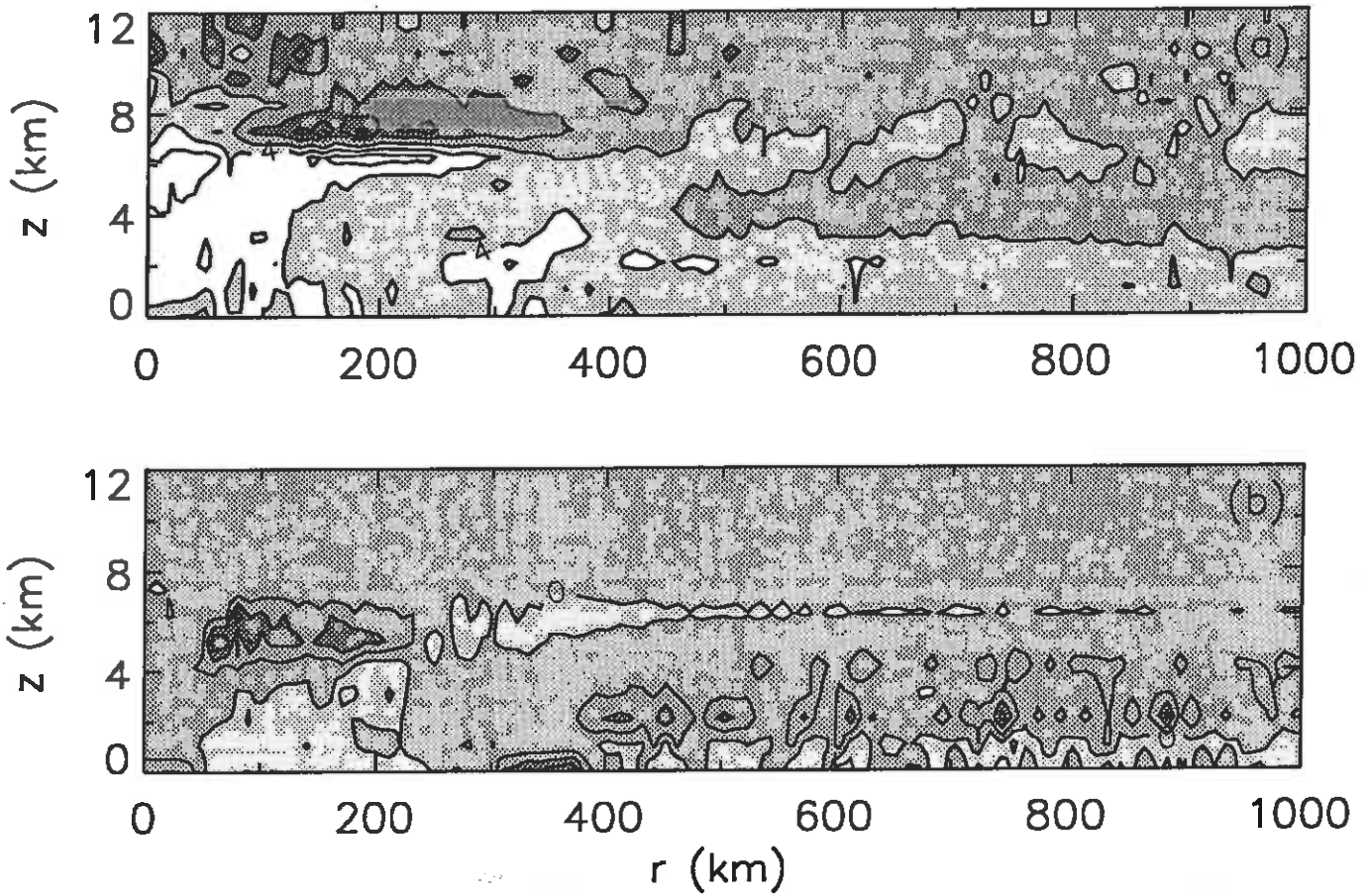


Figure 4. Radius-height sections for the control experiment, averaged from 40 to 50 hours, of local rate of change of potential temperature due to (a) advection, diffusion, and release of latent heat (contour interval 4 K day^{-1}), and (b) longwave radiation (contour interval 2 K day^{-1}). The shading is the same in (a) and (b), with dark gray denoting heating rates less than -4 K day^{-1} , medium gray heating rates between -4 and 0 K day^{-1} , and light gray heating rates from 0 to 4 K day^{-1} .

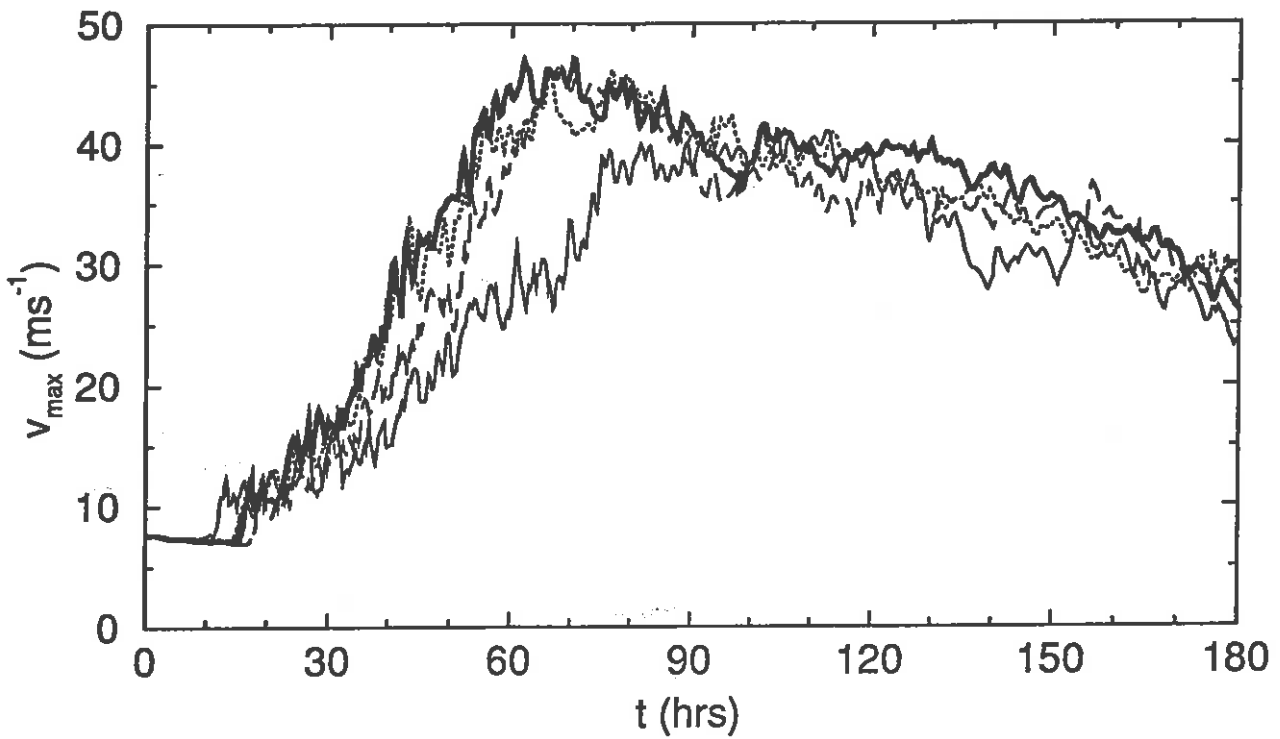


Figure 5. Maximum azimuthal wind speed as a function of time for the control simulation (thick solid line), no radiation (thin solid line), and simulations with saturation vapour pressure calculated over water (dashed line), and with cloud optical properties as for water (dotted line).

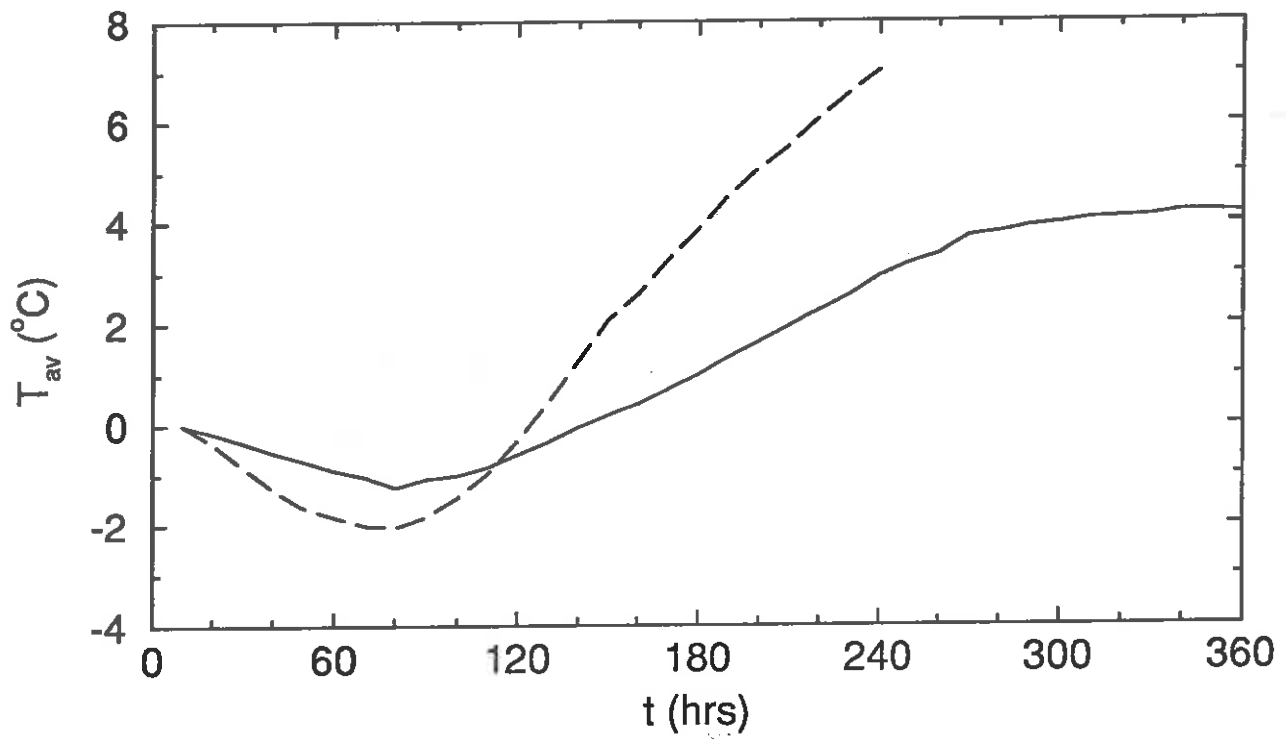


Figure 6. Deviation of temperature from its initial value, averaged over the region from 1500 to 2000 km in radius, and 0 to 8 km in height, for the control simulation (solid line), and an experiment using the microphysical parameterization of Emanuel and Rotunno (1989) (dashed line).

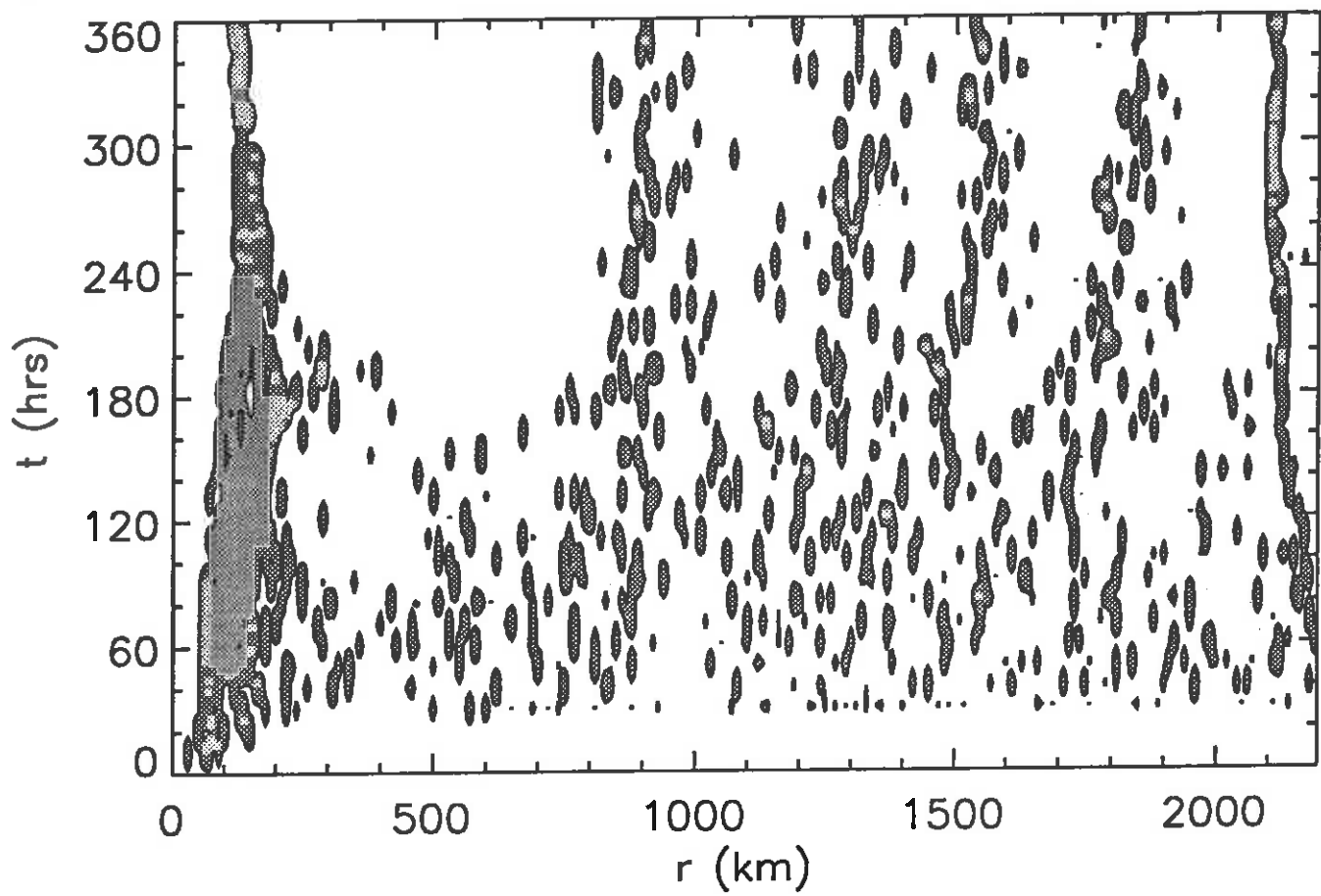


Figure 7. Region where ice concentration is greater than or equal to $2 \times 10^{-4} \text{ g kg}^{-1}$ at model level 2 ($z = 1.5 \text{ km}$), plotted as a function of radius and time.

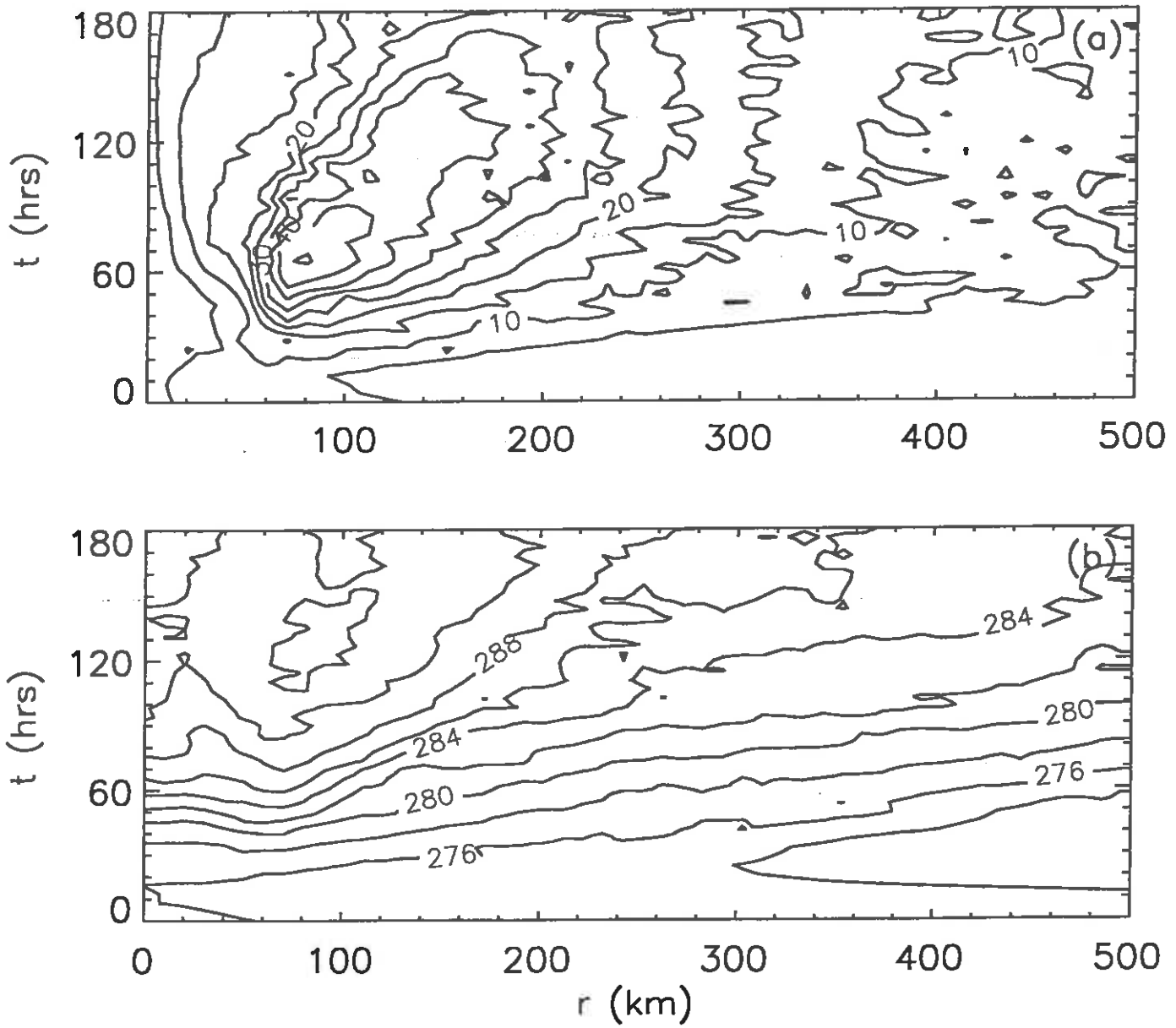


Figure 8. (a) Azimuthal velocity at model level 2 ($z = 1.5$ km) (contour interval 5 ms^{-1}), and (b) potential temperature at model level 4 ($z = 3.5$ km) (contour interval 2 K), plotted as functions of radius and time.

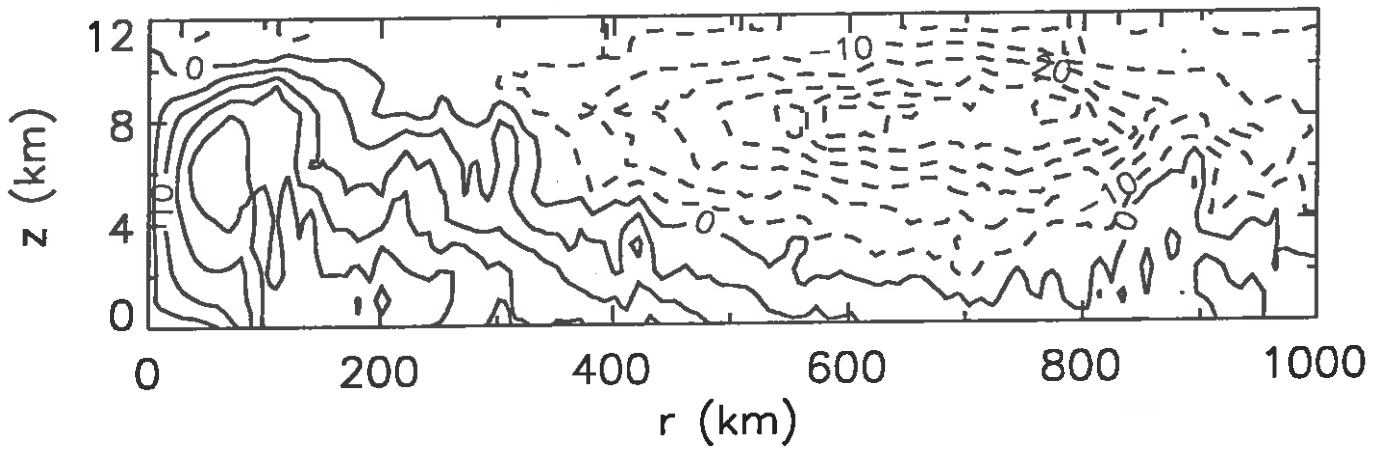


Figure 9. Radius-height section of azimuthal wind speed for the control experiment, at 40 hours (contour interval 5 ms^{-1} , dashed lines indicate negative values).

CURRENT JCMM INTERNAL REPORTS

This series of JCMM Internal Reports, initiated in 1993, contains unpublished reports and also versions of articles submitted for publication. The complete set of Internal Reports is available from the National Meteorology Library on loan, if required.

1. **Research Strategy and Programme.**
K A Browning et al
January 1993
2. **The GEWEX Cloud System Study (GCSS).**
GEWEX Cloud System Science Team
January 1993
3. **Evolution of a mesoscale upper tropospheric vorticity maximum and comma cloud from a cloud-free two-dimensional potential vorticity anomaly.**
K A Browning
January 1993
4. **The Global Energy and Water Cycle**
K A Browning
July 1993
5. **Structure of a midlatitude cyclone before occlusion.**
K A Browning and N Roberts
July 1993
6. **Developments in Systems and Tools for Weather Forecasting.**
K A Browning and G Szejwach
July 1993
7. **Diagnostic study of a narrow cold frontal rainband and severe winds associated with a stratospheric intrusion.**
K A Browning and R Reynolds
August 1993
8. **Survey of perceived priority issues in the parametrizations of cloud-related processes in GCMs.**
K A Browning
September 1993
9. **The Effect of Rain on Longwave Radiation.**
I Dharssi
September 1993
10. **Cloud Microphysical Processes - A Description of the Parametrization used in the Large Eddy Model.**
H Swann
October 1993

11. **An Appreciation of the Meteorological Research of Ernst Kleinschmidt.**
A J Thorpe
May 1992
12. **Potential Vorticity of Flow Along the Alps.**
A J Thorpe, H Volkert and Dietrich Heimann
August 1992
13. **The Representation of Fronts.**
A J Thorpe
January 1993
14. **A Parametrization Scheme for Symmetric Instability: Tests for an Idealised Flow.**
C S Chan and A J Thorpe
February 1993
15. **The Fronts 92 Experiment: a Quicklook Atlas.**
Edited by T D Hewson
November 1993
16. **Frontal wave stability during moist deformation frontogenesis. Part 1. Linear wave dynamics**
C H Bishop and A J Thorpe
May 1993
17. **Frontal wave stability during moist deformation frontogenesis. Part 2. The suppression of non-linear wave development.**
C H Bishop and A J Thorpe
May 1993
18. **Gravity waves in sheared ducts.**
S Monserrat and A J Thorpe
October 1993
19. **Potential Vorticity and the Electrostatics Analogy: Quasi-Geostrophic Theory.**
C Bishop and A J Thorpe
November 1993
20. **Recent Advances in the Measurement of Precipitation by Radar.**
A J Illingworth
April 1993
21. **Micro-Physique et Givrage. Cloud Microphysics and Aircraft Icing.**
A J Illingworth
May 1993

22. **Differential Phase Measurements of Precipitation.**
M Blackman and A J Illingworth
May 1993
23. **Estimation of Effective Radius of Cloud Particles from the Radar Reflectivity.**
N I Fox and A J Illingworth
May 1993
24. **A Simple Method of Dopplerising a Pulsed Magnetron Radar.**
L Hua, A J Illingworth and J Eastment
November 1993
25. **Radiation and Polar Lows.**
George C Craig
February 1994

Met Office Joint Centre for Mesoscale Meteorology Department of Meteorology
University of Reading PO Box 243 Reading RG6 6BB United Kingdom
Tel: +44 (0)118 931 8425 Fax: +44 (0)118 931 8791
www.metoffice.com

